

Article

Valve Stiction Detection Method Based on Dynamic Slow Feature Analysis and Hurst Exponent

Linyuan Shang ^{*}, Yuyu Zhang and Hanyuan Zhang

School of Information and Electrical Engineering, Shandong Jianzhu University, Jinan 250101, China

^{*} Correspondence: shanglinyuan20@sdjzu.edu.cn

Abstract: Valve stiction is the most common root of oscillation faults in process control systems, and it can cause the severe deterioration of control performance and system instability, ultimately impacting product quality and process safety. A new method for detecting valve stiction, based on dynamic slow feature analysis (DSFA) and the Hurst exponent, is proposed in this paper. The proposed method first utilizes DSFA to extract slow features (SFs) from the preprocessed and reconstructed data of the controller output and the controlled process variable; then, it calculates the Hurst exponent of the slowest SF to quantify its long-term correlation; and, finally, it defines a new valve detection index to identify valve stiction. The results obtained from simulations and actual process case studies demonstrate that the proposed method, based on a DSFA–Hurst exponent, can effectively detect valve stiction in control loops.

Keywords: valve stiction detection; process control; dynamic slow feature analysis; hurst exponent

1. Introduction

Control valves are widely applied in process control systems to regulate fluid flow, pressure, and temperature in various industrial processes, such as oil and gas, buildings, chemical, petrochemical, power, and water treatment. They are critical mechanical devices for the production process to achieve precise control and maintain product quality [1–3]. However, one of the challenges of control valve operation is the occurrence of stiction, which can lead to undesirable behavior, such as oscillations in the control loop, reducing its control performance and product quality. It also accelerates the wear and aging of valves and related equipment, and even causes system failure, resulting in safety accidents [4]. According to a survey, 20–30% of control loops experience oscillations due to valve failures caused by stiction or hysteresis [5]. In recent years, valve stiction detection has received much attention in academia and engineering due to its practical value in improving system reliability, control performance, and product quality.

The formal definition of valve stiction states that it is a characteristic of an element whereby its smooth motion in response to a changing input is preceded by a stationary phase, and then followed by a sudden, abrupt jump known as the “slip-jump”. This slip-jump in a mechanical system is caused by static friction that surpasses dynamic friction during smooth motion [6]. Several review articles and books on control valve stiction detection and quantification techniques have already appeared [2,7–9]. In the past decade, physics-based and data-driven-based methods have been developed to investigate the behavior of valve stiction. Physics-based methods utilize the first principles to describe the stiction phenomenon, providing a mechanistic understanding of valve behavior [10,11]. Di Capaci et al. proposed a method that utilizes the Hammerstein model and nonlinear optimization to accurately estimate the valve stiction parameters of a smoothed model for industrial processes controlled by model predictive controllers [12]. Romano and Garcia introduced a method that begins with an optimization-based approach in order to jointly estimate the friction and nonlinear process model parameters from closed-loop



Citation: Shang, L.; Zhang, Y.; Zhang, H. Valve Stiction Detection Method Based on Dynamic Slow Feature Analysis and Hurst Exponent. *Processes* **2023**, *11*, 1913. <https://doi.org/10.3390/pr11071913>

Academic Editors: Shuang-Hua Yang, Yi Cao and Yulong Ding

Received: 11 May 2023

Revised: 16 June 2023

Accepted: 23 June 2023

Published: 26 June 2023



Copyright: © 2023 by the authors. Licensee MDPI, Basel, Switzerland. This article is an open access article distributed under the terms and conditions of the Creative Commons Attribution (CC BY) license (<https://creativecommons.org/licenses/by/4.0/>).

tests. This method offers significant advantages when considering a nonlinear process model: improved accuracy in quantifying friction and reasonable estimates of the nonlinear steady-state characteristics of the process [13]. Based on power spectral density (PSD) and auto-correlation function (ACF), Karra and Karim proposed a model-based oscillation detection method to identify and quantify the root cause of oscillations [14]. However, implementing physics-based methods for control valves in ordinary differential equation (ODE) format poses several challenges. Firstly, the physical parameters, such as the mass of moving components and different friction forces, are difficult to measure. Secondly, these methods are invasive, which makes their implementation more challenging. Additionally, for industrial production processes with a large number of valves, establishing physical models can require significant human resources and cost expenses [4,15,16]. With the widespread use of distributed control systems (DCS), process data are generated and recorded in large quantities, giving rise to the data-driven-based approach. This approach does not require complex mechanisms and knowledge to detect faults from changes in process data. It is non-invasive and automatable, thus making it easier to implement [17].

Various data-driven-based methods have been proposed for detecting valve stiction in recent years, mainly in the following five categories: (1) correlation-based methods [18,19], (2) nonlinear-based methods [20,21], (3) waveform-shape-based methods [22,23], (4) limit-cycle-based methods [24,25], and (5) machine learning (ML)-based methods [16,26–28]. Among the above methods, Horch pioneered the development of the initial method for stiction detection [18]. This technique involves calculating the cross-correlation function between the controller output (OP) and controlled process variable (PV) data, and it is effective in detecting stiction in flow control loops. Choudhury et al. proposed a nonlinear-based approach to detect valve stiction. This approach identifies nonlinearities within a control loop by utilizing the sensitivity of the normalized bispectrum or bicoherence to potential nonlinear interactions in the control error signal [29]. Among the waveform-shape-based methods, a pattern recognition method, using the dynamic time warping (DTW) technique, was proposed by Srinivasan et al. This method can identify the different qualitative shapes caused by valve stiction from OP and PV data [5]. Garcia and Zakharov et al. proposed a valve detection system based on data characterizations to automatically select valve stiction detection algorithms. This system extracts different characterizations in the data by establishing different characterization indicators, and then automatically selects and applies the most suitable detection algorithm based on the analysis of the characterizations, which can effectively improve the detection performance and reliability [22,23]. Yamashita proposed a qualitative description formalism to describe qualitative trends or shapes of the valve input and output signals, then defined the stiction index to detect valve stiction patterns [30]. However, the traditional data-driven stiction detection methods mentioned above lack robustness when dealing with control loops with high noise and abnormal behavior [16].

Compared with the limitations of traditional data-driven methods, ML algorithms, such as convolutional neural network (CNN), have several advantages in the field of valve stiction detection. Firstly, ML algorithms typically perform feature extraction and are able to handle data with noise, thus showing better adaptability [31]. Secondly, with the widespread application of DCS in factories, the amount of available process data has increased immensely. This provides more training data for ML algorithms, thereby helping to improve detection accuracy. Furthermore, ML algorithms can generate efficient detection models through offline training. Once the model is trained, the computation time of ML will be significantly reduced, enabling faster computation in real-time applications [16,26]. Therefore, ML-based stiction detection methods have gained considerable attention from researchers in recent years. Amiruddin et al. proposed a stiction detection network (SDN) model to detect valve stiction. This model utilizes PV and OP as model inputs and trains a feed-forward neural network to build a stiction detection model [26]. The framework developed by Henry et al. used CNN and principal component analysis (PCA) to detect stiction and identify severity. The CNN is utilized to extract characteristics from the time series data of control valve actions, whereas the PCA is implemented to produce statistical process control maps derived from these

features, which enables automated monitoring of control valve stiction [27]. Kamaruddin et al. developed a simple butterfly-shape-based stiction detection (BSD) method that produces a unique “butterfly” pattern in the presence of valve stiction to quantify stiction severity [28]. Yazdi et al. applied support vector machines (SVM) to statistical variables constructed from OP and PV to detect valve stiction, and this method has the ability to distinguish between stiction and other sources of oscillation [32].

The above traditional data-driven stiction detection methods work under the assumption that the oscillation patterns in the control loop data are persistent and then detect the presence of specific periodic characteristics, autocorrelations, or power spectra [33]. Therefore, the above methods will be ineffective when stiction causes irregular oscillations in the control loop data. Among the ML-based stiction detection methods, the neural-network-based methods do not provide a comprehensive means to examine the influence resulting from the adjustment of stiction parameters between neurons, whether by augmentation or reduction [32]. PCA and SVM rely on the assumption that the data are temporally independent, disregarding the temporal dynamic properties in the data. However, the actual process system is dynamic [31], and valve stiction often leads to the nonlinear dynamic behavior of the process, which makes the process data exhibit strong long-term correlations. Unfortunately, the aforementioned methods rarely consider these two factors when detecting valve stiction.

This paper presents a ML approach for detecting valve stiction utilizing dynamic slow feature analysis (DSFA) and Hurst exponent, which considers the temporal dynamics and long-term correlation of process data. This method overcomes the constraints imposed by the assumptions of persistent oscillation patterns and the temporal independence of the data. The proposed method involves the preprocessing and reconstruction of OP and PV data from the control loop, followed by the application of DSFA to extract slow features (SFs) that capture the temporal dynamic characteristics of the single-lag in the reconstructed data. The Hurst exponent is utilized to measure the long-term correlation information of the slowest SF, which is then employed for valve stiction detection. This paper is structured as follows: Section 2 introduces the research problem of control valve stiction. Section 3 presents the theory and detailed steps of the proposed method. Section 4 presents the case study. Finally, Section 5 summarizes the conclusions drawn in this paper.

2. Valve Stiction

A typical control loop structure diagram is shown in Figure 1, where SP, OP, MV, and PV represent setpoint, controller output, valve position, and process output, respectively. Figure 2 shows the structure diagram of the valve [9,32,34]. On the basis of Newton’s second law, the force balance equation for the valve stem is as follows [9,15]:

$$Q \frac{d^2 g}{dt^2} = F_a + F_r + F_f + F_p + F_i \quad (1)$$

where Q and g denote the mass of the moving parts and the relative stem position, respectively. F_a , F_r , and F_f are the actuator applied force, the spring force, and the friction force of the valve, respectively. F_p is the force caused by fluid pressure drop and F_i is the extra force that maintains the valve in the seat. Within the realm of forces under consideration, F_p and F_i are ascribed a value of zero, owing to their insubstantial influence, while the friction force F_f emerges as the pivotal determinant governing the dynamics of the valve [15].

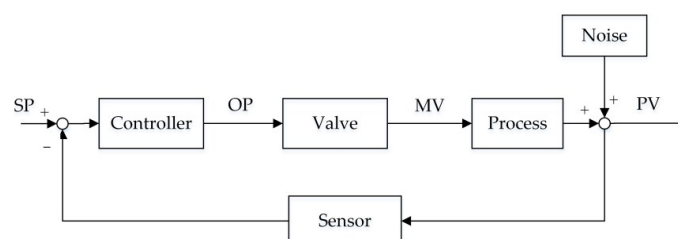


Figure 1. Control loop structure.

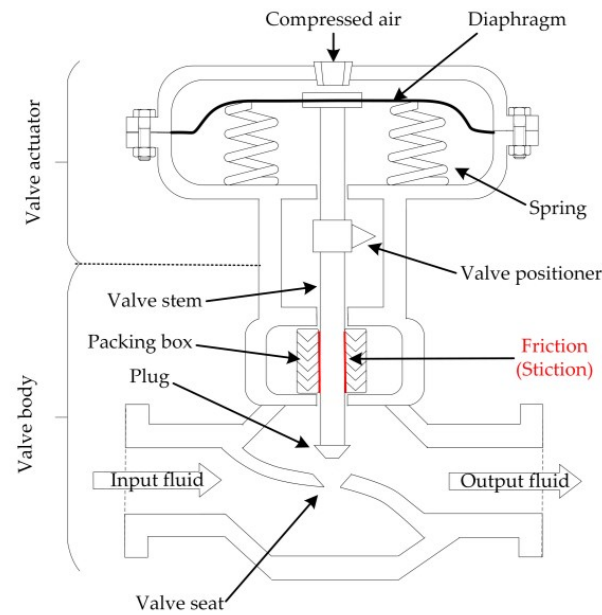


Figure 2. The structure diagram of the valve.

Valve stiction is one of the main causes of control loop oscillations. This phenomenon is that the valve stem cannot move due to static friction when it is stressed, and the valve stem slips and jumps after overcoming the static friction force [6]. According to the two-parameter valve model defined by Choudhury, two parameters, S and J , are used to describe valve stiction [6]. The OP-MV phase diagram of the valve under this model is shown in Figure 3, where $S = \text{stick} + \text{deadband}$ and $J = \text{stickband}$.

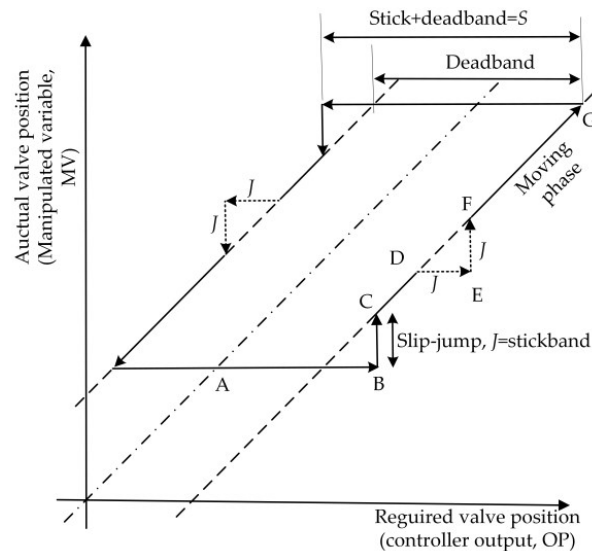


Figure 3. OP-MV characteristic of a sticky valve.

Figure 4 shows OP-MV and OP-PV plots with a sticky control valve. From Figure 4a, it can be seen that, affected by the static friction of the valve, the OP-MV plot presents a limit cycle shape instead of a linear relationship in the normal state. Similarly, OP-PV in Figure 4b is also a limit cycle shape. Since the variable MV in most actual control loops is difficult to measure [34], the proposed method uses OP and PV data to detect valve static friction, which is more practical. Figure 5 shows the OP and PV curves with a sticky control valve, taken from a simple numerical simulation example. The X-axis represents the oscillation magnitude of OP and PV with respect to the steady-state point of the system, and the Y-axis is the number of samples in time order.

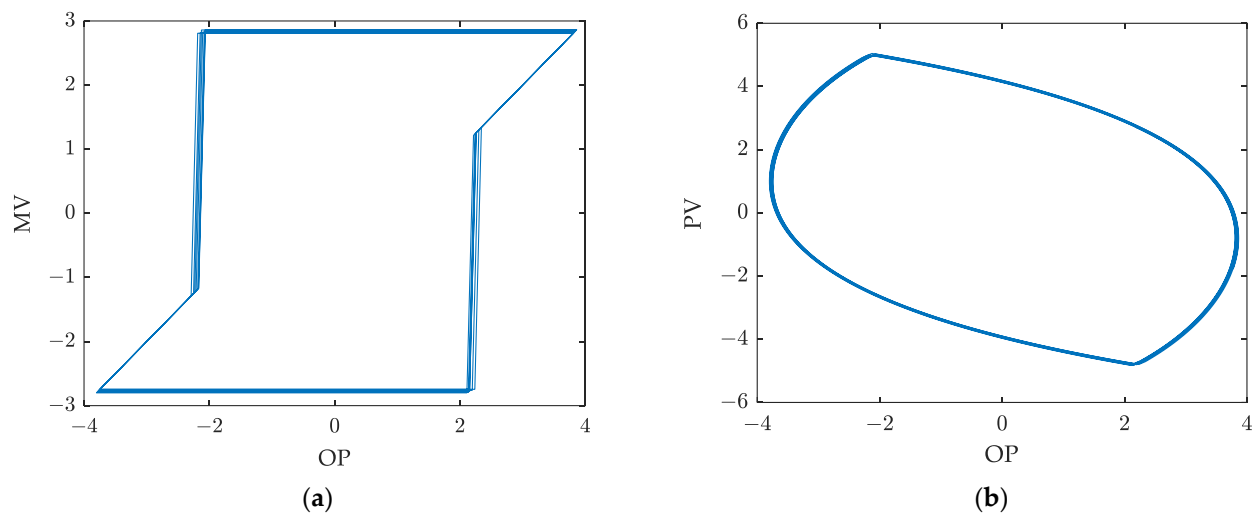


Figure 4. OP-MV and OP-PV plots with a sticky control valve: (a) OP-MV plot; (b) OP-PV plot.

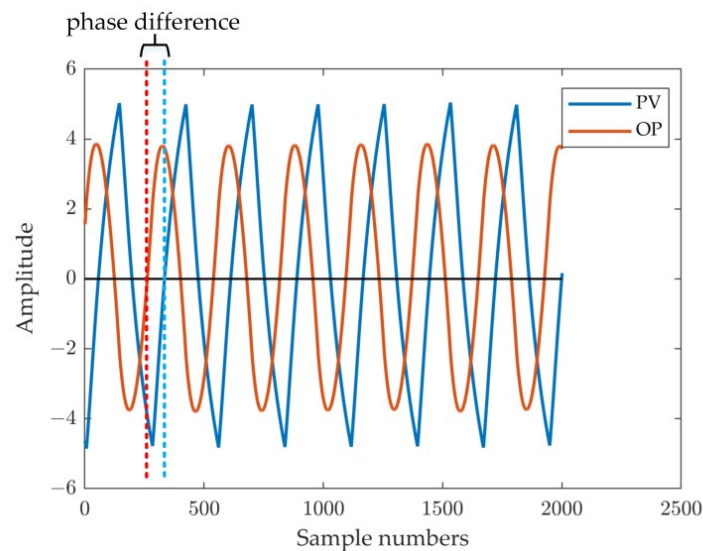


Figure 5. OP and PV curves with a sticky control valve.

3. Methodology

This section contains the principle and the steps of the proposed method in detail. Firstly, the OP and PV data were preprocessed and reconstructed. Then, the SFs of the reconstructed data were extracted by the DSFA method, and the long-term correlation of the slowest SF sequence was calculated by the Hurst exponent. Finally, a new valve detection index was defined.

3.1. Data Preprocessing and Reconstruction

In this step, the collected data were subjected to standardization preprocessing and reconstruction. Magnitude issues often arise due to variations in variable units and the nature of the process. To prevent bias in subsequent analysis, it was imperative to establish a consistent scaling magnitude for each data set [35]. Therefore, the OP and PV data were standardized to zero mean and unit variance, respectively, according to Equation (2):

$$v(k) = \frac{x(k) - \bar{x}}{\sigma} \quad (2)$$

where $x(k)$ ($k = 1, \dots, N$) represent N time series samples, and \bar{x} and σ are the mean and sample standard deviation of time series samples.

As can be seen from Figure 5, PV and OP exhibited periodic oscillations with a certain phase difference after static friction occurred in the valve. Therefore, we used the difference between PV and OP, which also had periodic oscillation characteristics, to construct a new time series for detecting valve stiction.

$$d(k) = v_{PV}(k) - v_{OP}(k) \quad (3)$$

where $v_{PV}(k)$ and $v_{OP}(k)$ are standardized time series PV and OP, respectively.

3.2. Dynamic Slow Feature Analysis

3.2.1. Slow Feature Analysis

As an up-and-coming ML algorithm, slow feature analysis (SFA) has been widely applied in control performance evaluation [36,37] and the detection of process faults [38–41]. SFA is mainly used to extract SFs from time series data $\mathbf{x}^T(t) = [x_1(t), x_2(t), \dots, x_M(t)]$, and the goal of SFA is to find a set of mapping functions $\mathbf{q}^T(t) = [q_1(t), q_2(t), \dots, q_M(t)]$, whose output has the largest single-lag autocorrelation [42]. The objective function of SFA is:

$$\min \langle \dot{\mathbf{s}}_j^2 \rangle_t \quad (4)$$

and the constraints are as follows:

$$\langle \mathbf{s}_j \rangle_t = 0 \quad (5)$$

$$\langle \mathbf{s}_j^2 \rangle_t = 1 \quad (6)$$

$$\forall i \neq j, \langle \mathbf{s}_i \mathbf{s}_j \rangle_t = 0 \quad (7)$$

where $\dot{\mathbf{s}}_j(t) = \mathbf{s}_j(t) - \mathbf{s}_j(t-1)$, $\langle \cdot \rangle_t$ is time averaging and is defined as:

$$\langle f \rangle_t = \frac{1}{t_1 - t_0} \int_{t_0}^{t_1} f(t) dt \quad (8)$$

The SFs extracted by SFA are sorted from slow to fast, that is, s_1 is the slowest feature, s_2 is the second, and so on. Linear SFA represents these features as a linear combination of time series data columns. The corresponding equation is given as

$$\mathbf{s} = \mathbf{W}\mathbf{x} \quad (9)$$

where $\mathbf{W} = [w_1, \dots, w_M]^T$ is the transformation matrix, and $w_j (j = 1, \dots, M)$ denotes coefficient vector. \mathbf{W} can be obtained by solving the following generalized eigenvalue problem:

$$\mathbf{A}\mathbf{W} = \mathbf{B}\mathbf{W}\mathbf{\Omega} \quad (10)$$

where $\mathbf{A} = \langle \dot{\mathbf{x}}\dot{\mathbf{x}}^T \rangle_t$, $\mathbf{B} = \langle \mathbf{x}\mathbf{x}^T \rangle_t$, and $\mathbf{\Omega} = \text{diag}\{\omega_1, \dots, \omega_M\}$ is a diagonal matrix of generalized eigenvalues. The solution to the above generalized eigenvalue problem is summarized below:

1. Standardized input data to zero mean and unit variance, $\tilde{\mathbf{x}}$;
2. Singular value decomposition (SVD) is employed on the covariance matrix of $\tilde{\mathbf{x}}$ in order to obtain spherical data \mathbf{Z} .

$$\langle \tilde{\mathbf{x}}\tilde{\mathbf{x}}^T \rangle_t = \mathbf{U}\mathbf{A}\mathbf{U}^T \quad (11)$$

$$\mathbf{Z} = \mathbf{A}^{-1/2}\mathbf{U}^T\tilde{\mathbf{x}} \quad (12)$$

By applying SVD to the covariance matrix of \mathbf{Z} , \mathbf{W} can be computed as follows:

$$\langle \dot{\mathbf{Z}}\dot{\mathbf{Z}}^T \rangle_t = \mathbf{P}\mathbf{\Omega}\mathbf{P}^T \quad (13)$$

$$\mathbf{W} = \mathbf{P}\mathbf{A}^{-1/2}\mathbf{U}^T \quad (14)$$

3.2.2. Dynamic SFA

In order to better extract the dynamic features in the oscillating time series, the input data of SFA were further expanded using l lag samples to derive a dynamic SFA (DSFA) [37]. Meanwhile, through data expansion, $d(k)$, which is the input of SFA, was expanded from a single-dimensional vector to a multi-dimensional matrix, which matched the SFA algorithm. The data matrix is stacked as shown in Equation (15):

$$D_d(k) = \begin{bmatrix} d(k) & d(k-1) & \cdots & d(k-l) \\ d(k+1) & d(k) & \cdots & \\ \vdots & \vdots & \ddots & \vdots \\ d(k+n-1) & d(k+n-2) & \cdots & d(k+n-l-1) \end{bmatrix} \quad (15)$$

where $D_d(k)$ is the stacked matrix.

According to the SFA principle, the slowest SF corresponds to the smallest generalized eigenvalue, and the smaller the eigenvalue, the stronger the single-lag autocorrelation of the extracted SF. In the proposed method, we estimated the Hurst exponent for the slowest SF. In order to ensure that the slowest SF could more fully extract dynamic features, we selected the l value when the ratio of the generalized eigenvalue of the slowest SF to the sum of the generalized eigenvalues of all SFs was less than 5%.

The oscillation signal due to valve stiction had high autocorrelation, and DSFA was able to extract the largest single-lag autocorrelation of the oscillation signal. In addition, the lagged autocorrelation of some noise was zero, indicating that DSFA mitigated the effect of noise to some extent [41]. Therefore, we chose the slowest SF s_1 to detect valve stiction.

3.3. Hurst Exponent

The DSFA method only extracts the dynamic feature information of single-lag, and in order to further extract the long-term correlation information, the Hurst exponent was used to analyze the slowest SF s_1 . The Hurst exponent can quantify the extent of long-term correlation in a time series, where the influence of current or past values of the series extends significantly into the future. This influence surpasses what random fluctuations alone can produce. The Hurst exponent is capable of detecting and analyzing nonlinear dynamics in systems and has been widely used in financial market analysis [42], controller performance evaluation [43], and hydrological data analysis [44].

The detrended fluctuation analysis (DFA) algorithm is a very effective method for estimating the Hurst exponent of a time series $x(k)$, ($k = 1, \dots, N$), and it is divided into the following steps [43]:

1. Calculate a cumulative time series $X(i)$ by following equation:

$$X(i) = \sum_{k=1}^i (x(k) - \bar{x}) \quad i = 1, 2, \dots, N \quad (16)$$

where \bar{x} is the mean of $x(k)$;

2. Split $X(i)$ into d non-overlapping windows of length n , each of which is then fitted with a first-order least-squares line $\hat{X}_j(i)$, $j = 1, \dots, d$;
3. Calculate the variance f_j^2 for each window as follows:

$$f_j^2 = \frac{1}{n} \sum_{i=1}^n (X_j(i) - \hat{X}_j(i))^2, \quad j = 1, \dots, d \quad (17)$$

4. The calculation of the root mean square fluctuation should be performed as a function of the window size by:

$$F(n) = \sqrt{\frac{1}{d} \sum_{j=1}^d f_j^2} \quad (18)$$

5. Perform steps 2–4 repeatedly with varying window lengths n ;

6. Plot $F(n)$ versus n on a log-log graph. Determine the slope of this log-log graph, which represents an approximation of the Hurst exponent, denoted as He .

In the case of a time series, the value He varied from 0 to 1. If He was close to 0.5, it indicated that the long-term correlation of the time series approaches zero; on the contrary, if He was far from 0.5, it indicated that the time series had long-term persistence/positive correlation, i.e., there were potential nonlinear dynamics in the system [43,44].

3.4. Stiction Detection Index and Algorithm Steps Based on DSFA-Hurst Exponent

Inspired by the performance evaluation method [43], the stiction detection index H_s is defined as:

$$H_s = \begin{cases} He/0.5 & \text{if } He \leq 0.5 \\ (1 - He)/0.5 & \text{if } He > 0.5 \end{cases} \quad (19)$$

H_s values range from 0 to 1, with values closer to 0 indicating higher long-term correlation in the time series, which is a sign of valve stiction. A threshold of 0.5 was used in this paper to diagnose valve stiction. If H_s was less than 0.5, it indicated that a valve stiction fault had occurred.

Figure 6 depicts the flowchart of this algorithm. The detailed steps are as follows:

1. Collect OP and PV data from DCS;
2. Standardize the collected OP and PV according to Equation (2);
3. Use Equations (3) and (15) to calculate the difference between OP and PV, and stack the difference to obtain D_d ;
4. Use the DSFA algorithm in Section 3.2 to extract the slowest SF s_1 of D_d ;
5. Calculate the Hurst exponent He of the slowest SF s_1 using the DFA method in 3.3;
6. Calculation of valve stiction index H_s using the Equation (19).

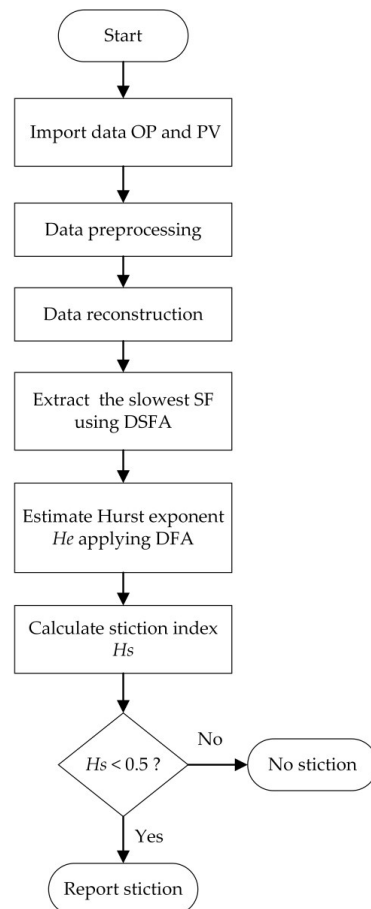


Figure 6. Flowchart of the proposed valve stiction index based on DSFA–Hurst exponent.

4. Case Study

In this section, the proposed H_s index is tested and compared with the R index in three different scenarios, including the benchmark numerical simulation of a simple control loop [4,31], a mixed-model simulation of a continuous stirred tank heater (CSTH) benchmark system [45], and the real process data from an international stiction database (ISDB) [9]. The R index is a classical method for detecting persistent oscillations using zero-crossings of the ACF and has been used to detect valve stiction [19,35].

$$R = \frac{1}{3} \left(\frac{T_p}{\sigma_{T_p}} \right) \quad (20)$$

where T_p and σ_{T_p} are the mean and standard deviation of the ACF oscillation period, respectively. If $R > 1$, this indicates that the control loop has regular oscillation, which may be caused by valve stiction or by persistent external disturbance. The two-parameter valve model, as defined by Choudhury, which is presented in Section 2, is used in Scenario one and Scenario two.

4.1. Scenario One

In this scenario, the proposed H_s index is tested on a benchmark numerical simulation process; the process model and controller transfer functions are given by Equations (21) and (22) [4,31]:

$$G_p = \frac{3}{10s + 1} e^{-10s} \quad (21)$$

$$G_c = 0.2 \times \frac{10s + 1}{10s} \quad (22)$$

where the simulation step interval is 0.1, and the number of samples is 2000. The noise a_t follows a standard Gaussian distribution and $a_t \sim N(0, 0.5^2)$.

Figure 7 shows the oscillation curves and limit cycle plots with the valve stiction parameter $S = 2$, $J = 1$. It can be seen from the curves in Figure 7a that both v_{PV} and v_{OP} exhibit a periodic oscillation trend, and there is a phase gap between them, so their difference signal d presents a periodic oscillation. From the plots in Figure 7b, $v_{OP}-d$ and $v_{OP}-v_{PV}$ are both limit cycle shapes, which shows the presence of nonlinearity between v_{OP} and d , just like that between v_{OP} and v_{PV} .

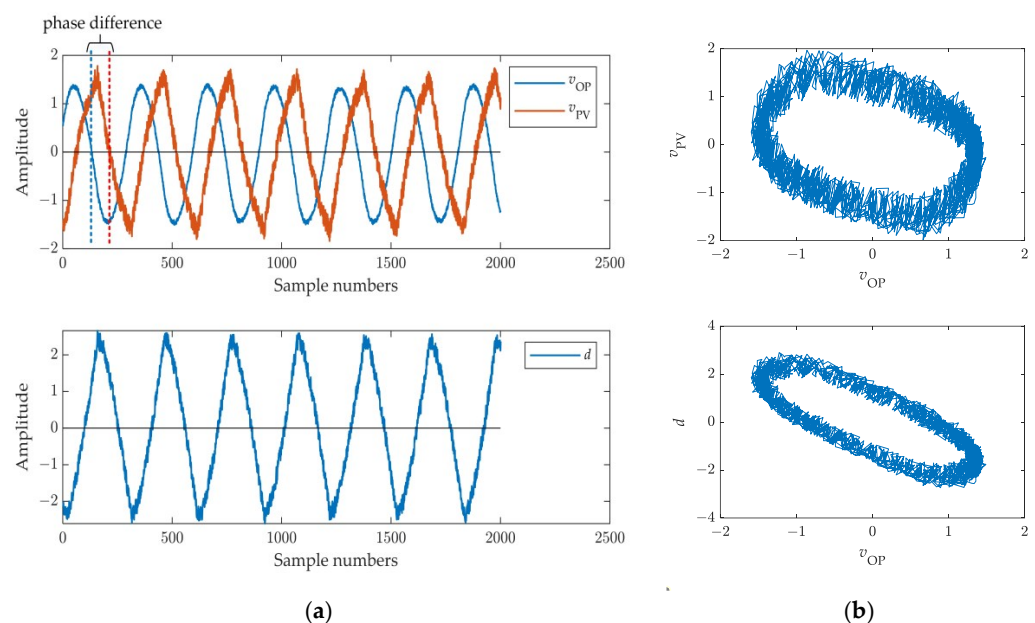


Figure 7. Oscillation curves and limit cycle plots with sticky control valve when parameters $S = 2$ and $J = 1$: (a) oscillation curves of v_{OP} , v_{PV} , and d ; (b) limit cycle plots of $v_{OP}-v_{PV}$ and $v_{OP}-d$.

Table 1 lists the detection results under five valve stiction parameters in the numerical simulation process. It can be observed that, for all five cases, the H_s indices of the proposed method were less than 0.5, indicating the presence of valve stiction. Similarly, the R indices were also greater than 1, indicating the detection of oscillations in the loop resulting from valve stiction.

Table 1. The detection results of H_s index and R index under five valve stiction parameters.

Case	R	H_s
$S = 2, J = 1$	75.9120	0.4383
$S = 2, J = 1.5$	13.4174	0.2988
$S = 2, J = 2$	83.0315	0.1232
$S = 2, J = 2.5$	18.8464	0.2458
$S = 2, J = 3$	26.8159	0.2850

Table 2 lists the detection results under external unit step disturbance and different sinusoidal disturbances in the numerical simulation process. The sinusoidal disturbance signal expression is shown in Equation (23):

$$E_d = A \times \sin(\omega t) \quad (23)$$

where A and ω are the amplitude and frequency of the sinusoidal disturbance signal, respectively. From the results, it can be seen, that when a unit step disturbance is introduced, $R = 0.4963$, which is less than 1. This indicates that no oscillation occurs in the loop in this case, and the result is correct. For other cases, when sinusoidal disturbance signals are added, the values of R are greater than 1, indicating oscillations occur in the loop. When $A = 1$ and $\omega = 3$, $H_s = 0.2861$, which is less than 0.5. This indicates the presence of valve stiction in this case, and the result is incorrect. The values of H_s in other cases are greater than 0.5, indicating the absence of valve stiction, which aligns with the simulation cases.

Table 2. The detection results of H_s index and R index under external step disturbance and sinusoidal disturbances.

Case	R	H_s
unit step disturbance	0.4963	0.7410
$A = 1, \omega = 3$	19.9481	0.6550
$A = 3, \omega = 3$	6.7425	0.7082
$A = 5, \omega = 3$	5.9312	0.7317
$A = 3, \omega = 2$	19.5162	0.2861
$A = 3, \omega = 4$	45.5180	0.9590

4.2. Scenario Two

The CSTD benchmark process is a heat exchanger system commonly applied in chemical process fault diagnosis [46–48] and safety analysis [49]. Its dynamic model describes the behavior of the CSTD system in terms of fluid flow, heat transfer, and temperature dynamics. Thornhill et al. employ a combination of measured data extracted from a process and a physical mechanism model, developing a hybrid model [45]. It incorporates the detailed characterization of valves, sensors, and the heat exchanger, resulting in more sophisticated and realistic features. Refer to Figure 8 for its structural representation. In the experiment, u_1 and u_2 were treated as manipulated variables, while y_1 and y_3 were considered as controlled variables. Specifically, y_1 was controlled by u_1 , while y_3 was controlled by u_2 .

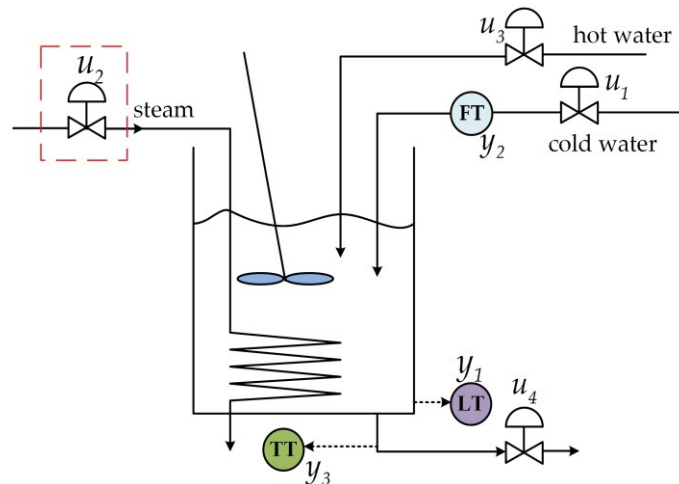


Figure 8. The structure of CSTD.

The following displays the dynamic volumetric and heat balances of the CSTD:

$$\frac{dV(l)}{dt} = f_{cw} + f_{hw} - f_{out}(l) \quad (24)$$

$$\frac{dH}{dt} = W_{st} + h_{hw}\rho_{hw}f_{hw} + h_{cw}\rho_{cw}f_{cw} - h_{out}\rho_{out}f_{out}(l) \quad (25)$$

Table 3 provides a description of the parameters for the CSTD system, and Table 4 displays the operational situation. In this case, the simulation step interval is 1, the number of samples is 2000. The noise ε_t follows a standard Gaussian distribution and $\varepsilon_t \sim N(0, 0.4^2)$. The PI controller parameters for the temperature control loop are $K_p = 1.5$ and $T_i = 0.04$. The steam valve u_2 is set with stiction, resulting in temperature oscillation inside the tank.

Table 3. Description of parameters for CSTD.

Parameter	Description	Parameter	Description
u_1	Input of the steam valve	u_2	Input of the cold water valve
u_3	Input of the hot water valve	u_4	Input of the water outlet valve
y_1	Level	y_3	Temperature
V	The volume of water	h_{hw}	The specific enthalpy of hot water feed
l	The level of water	h_{cw}	The specific enthalpy of cold water feed
f_{cw}	The cold water flow into the tank	ρ_{hw}	The density of incoming hot water
f_{hw}	The hot water flow into the tank	ρ_{cw}	The density of incoming cold water
f_{out}	The outflow from the tank	ρ_{out}	The density of water leaving the tank
H	The total enthalpy in the tank	W_{st}	The heat inflow from steam

Table 4. The operational situation of the CSTD system.

Variable	Operating Point
Temperature	42.52 °C
Level	20.48 cm
Steam valve	12.57 mA
Cold water valve	12.96 mA
Cold water flow	90.38 cm ³ /s
Hot water flow	0 cm ³ /s
Hot water valve	0 mA

The oscillation curves and limit cycle plots with the valve stiction parameter $S = 1$, $J = 0.5$ are shown in Figure 9. From the curves in Figure 9a, we find that both v_{u_2} and v_{y_3} oscillate, but the oscillations are not periodic and have a certain randomness. There is also a phase difference between the two. Hence, the signal d also exhibits irregular oscillation. In Figure 9b, the limit cycle shapes, plotted by $v_{u_2}-v_{y_3}$ and $v_{u_2}-d$, also display irregular patterns, indicating the presence of nonlinearity.

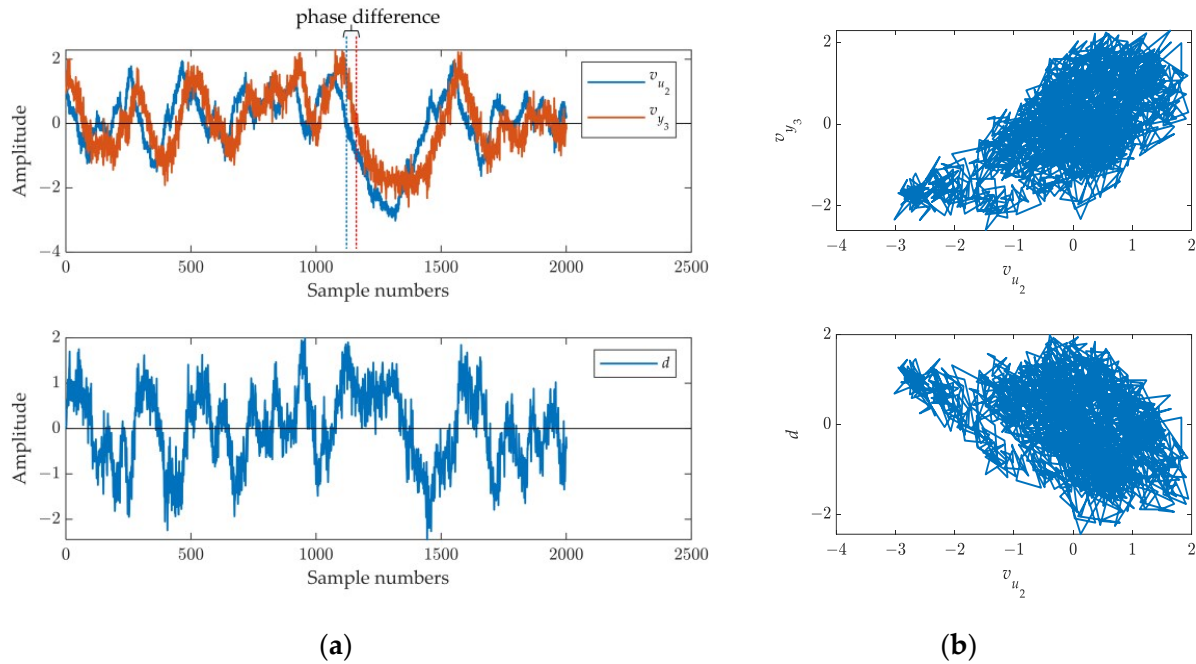


Figure 9. Oscillation curves and limit cycle plots with sticky control valve when parameters $S = 1$ and $J = 0.5$: (a) oscillation curves of v_{u_2} , v_{y_3} , and d ; (b) limit cycle plots of $v_{u_2}-v_{y_3}$ and $v_{u_2}-d$.

The detection results under different valve stiction parameters are presented in Table 5. It can be noted that the H_s indices were below 0.5 for all five cases, indicating the presence of valve stiction. However, the R indices were less than 1, indicating that no oscillations were detected and these results were failures. Figure 10 provides the ACF curves of the system output when the parameters $S = 1$, $J = 0.5$ in Scenario two, and the parameters $S = 2$, $J = 1$ in Scenario one. Compared with the ACF in Scenario one shown in Figure 10b, the intervals between the ACF zero-crossing points of the irregular oscillation time series also have a certain degree of randomness, as shown in Figure 10a. This is the reason for the detection failure of the R index. Meanwhile, the proposed method calculated the long-term correlation over the entire sample data range, and therefore accurately detected this irregular oscillation signal, i.e., the valve stiction was successfully detected. According to the experimental results mentioned above, the proposed method had better detection performance when valve stiction led to irregular oscillation.

Table 5. The detection results of the proposed H_s index and R index under five valve stiction parameters.

Case	R	H_s
$S = 1, J = 0.5$	0.1786	0.2255
$S = 1, J = 0.75$	0.1296	0.3265
$S = 1, J = 1$	0.0810	0.2938
$S = 1, J = 1.25$	0.0919	0.2130
$S = 1, J = 1.5$	0.1748	0.2696

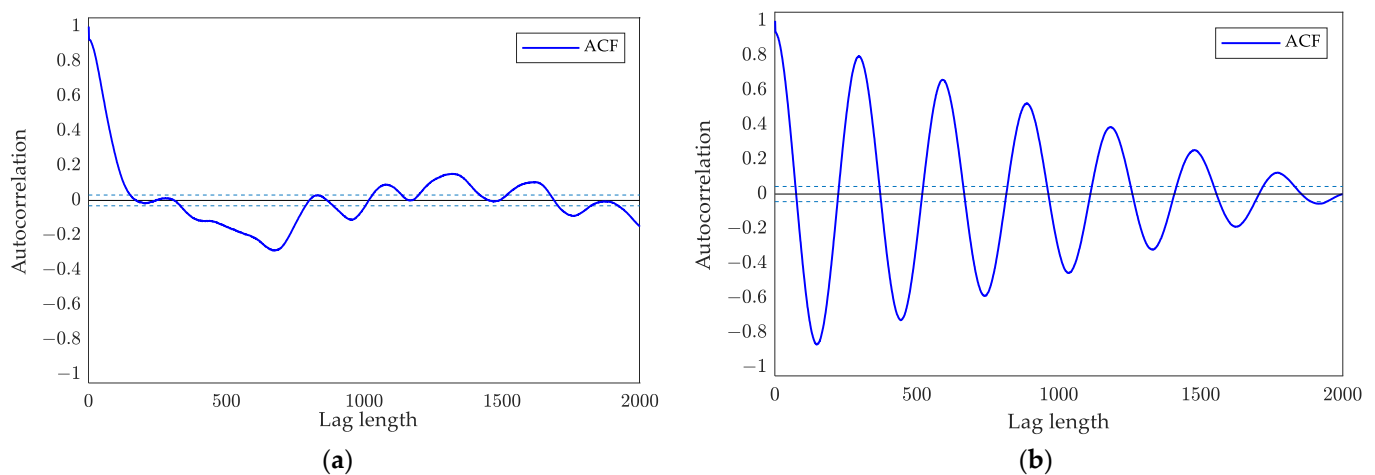


Figure 10. ACF of the system output: (a) with the parameters $S = 1, J = 0.5$ in Scenario two; (b) with the parameters $S = 2, J = 1$ in Scenario one.

Table 6 presents the detection results in CSTH under external unit step disturbance and various sinusoidal disturbances. Upon examining the results, it is evident that when a unit step disturbance was added, $R = 0.3045$, which was less than 1. This suggests that no oscillation occurred in the loop in this case, yielding a correct outcome. Conversely, in the remaining cases, where sinusoidal disturbance signals were added, the R values exceeded 1, indicating the presence of oscillations in the loop. For valve detection index H_s , when $A = 1$ and $\omega = 0.75$, $H_s = 0.4093$, which falls below 0.5. This signifies the existence of valve stiction in this case, rendering the result inaccurate. Conversely, the H_s values surpassed 0.5 in other cases, denoting the absence of valve stiction, thus aligning with the simulated cases.

Table 6. The detection results of H_s index and R index under external step disturbance and sinusoidal disturbances.

Case	R	H_s
unit step disturbance	0.3045	0.6988
$A = 0.5, \omega = 0.5$	31.6027	0.8209
$A = 1, \omega = 0.5$	39.1983	0.7796
$A = 1.5, \omega = 0.5$	57.6984	0.7626
$A = 1, \omega = 0.75$	52.2941	0.4093
$A = 1, \omega = 0.25$	56.2201	0.5388

4.3. Scenario Three

The real process data, provided by ISDB under the valve stiction faults in temperature control loop 6 and loop 7 in buildings, are used in this section, and control loop 6 and loop 7 are abbreviated as 'Buildings-6' and 'Buildings-7', respectively.

Figures 11 and 12 show the oscillation curves and limit cycle plots of Buildings-6 and Buildings-7. It can be observed that the two cases had periodic oscillation due to the valve stiction, and there was a phase difference between OP and PV. In addition, the OP and PV plots were the limit cycle shapes, indicating that both loops had severe nonlinearity. The detection results in Table 7 show that the proposed method successfully detected valve stiction. Additionally, the method based on R index also detected loop oscillations caused by valve stiction.

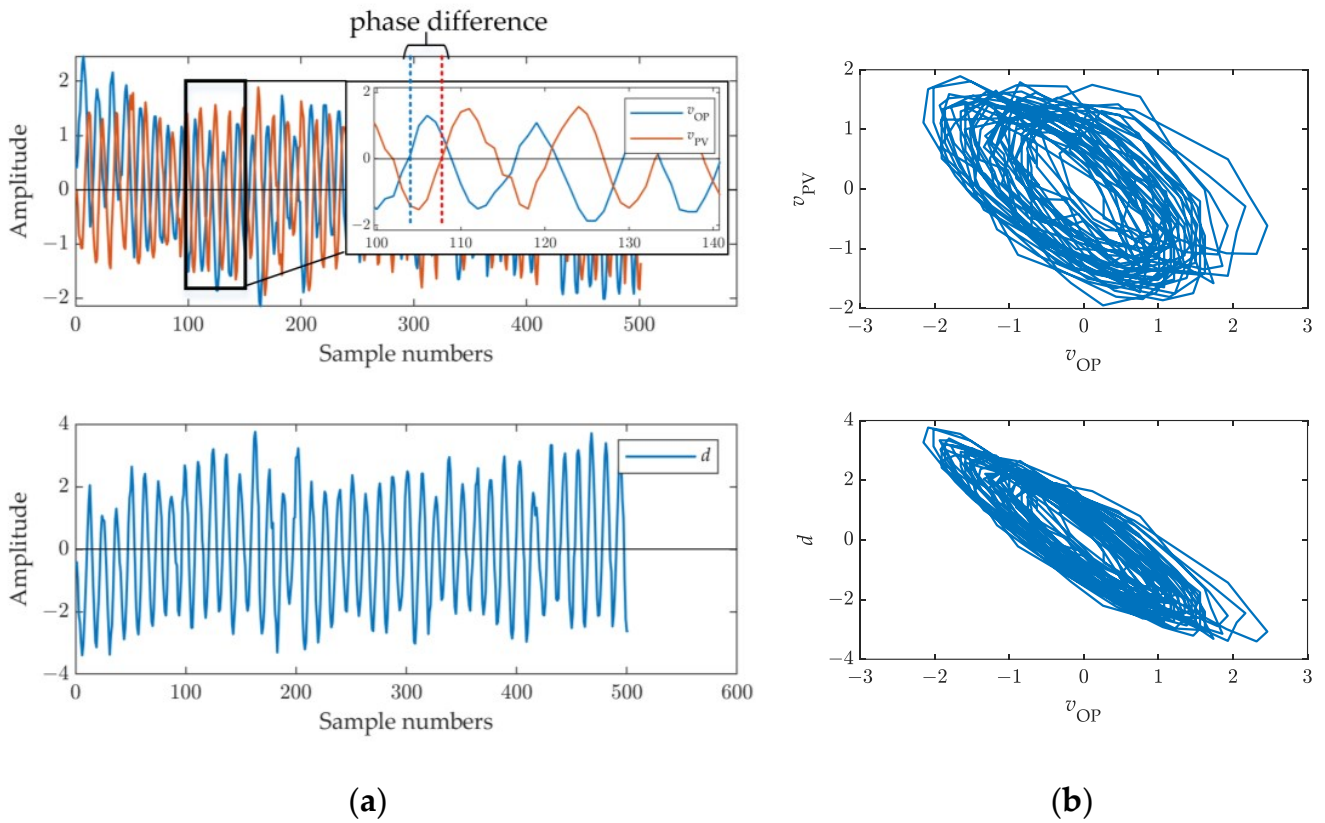


Figure 11. Oscillation curves and limit cycle plots with sticky control valve of Buildings-6: (a) oscillation curves of v_{OP} , v_{PV} , and d ; (b) limit cycle plots of v_{OP} - v_{PV} and v_{OP} - d .

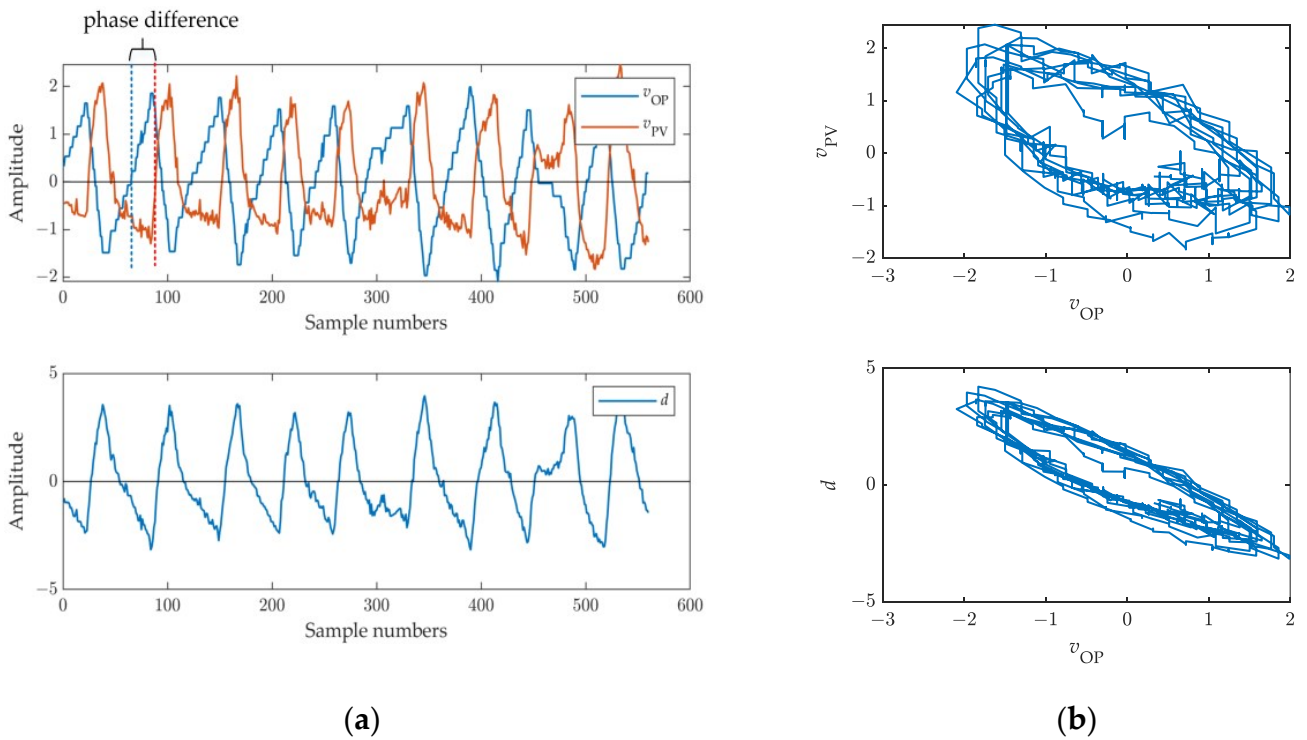


Figure 12. Oscillation curves and limit cycle plots with sticky control valve of Buildings-7: (a) oscillation curves of v_{OP} , v_{PV} and d ; (b) limit cycle plots of v_{OP} - v_{PV} and v_{OP} - d .

Table 7. The detection results of the proposed H_s index and R index of Buildings-6 and Buildings-7.

Case	R	H_s
Buildings-6	4.4380	0.3719
Buildings-7	5.4544	0.3361

The comprehensive experimental results led to the conclusion that the proposed H_s index can effectively detect valve stiction. By considering the temporal dynamic characteristics and long-term correlation information of the process data, the method was also accurate in detecting non-periodic random oscillations caused by static friction and exhibited a better performance compared with the R index. Meanwhile, through simulation tests on external sinusoidal disturbances of different amplitudes and frequencies, it was observed that the proposed H_s index had a certain ability to distinguish between valve stiction and external sinusoidal disturbances. However, it also had false alarms, meaning that it incorrectly identified external sinusoidal disturbance as valve stiction.

The proposed method has its limitations. Firstly, the method requires a phase difference between OP and PV data. Secondly, the calculation of the Hurst exponent requires an adequate number of samples to ensure accuracy, thus making it unsuitable for datasets with small sample sizes. Thirdly, the proposed method may generate false alarms in detecting external sinusoidal disturbances. To reduce such false alarms, it can be combined with other methods such as cross-correlation function or SVM. Alternatively, further research and improvement in the proposed method are needed to achieve this goal, which will be our future research work.

5. Conclusions

In this paper, an ML method for valve stiction detection based on the DSFA–Hurst exponent is proposed, aiming to detect valve stiction by utilizing dynamic features and long-term correlation information in process data. This method mainly involves two layers of ML algorithms: in the first layer, the DSFA method is implemented to extract the SFs, which can characterize the slow change information from the differential reconstruction data between the OP and the PV. Then, in the second layer, the long-term correlation of the slowest SF information is calculated based on the Hurst exponent. Finally, a new valve stiction detection index H_s is defined. The experimental results indicate that the proposed method can effectively detect the stiction of the valve, even when the valve stiction causes irregular oscillations. It also demonstrates a certain capability to differentiate between valve stiction and external sinusoidal disturbances.

Author Contributions: Conceptualization, L.S.; formal analysis, H.Z.; funding acquisition, H.Z.; methodology, L.S.; project administration, L.S.; resources, L.S.; software, Y.Z.; supervision, H.Z.; validation, L.S., Y.Z. and H.Z.; visualization, Y.Z.; writing—original draft, L.S. and Y.Z.; writing—review and editing, L.S. and H.Z. All authors have read and agreed to the published version of the manuscript.

Funding: This research was funded by the Youth Innovation Team Technology Project of the Higher School in Shandong Province, grant number 2022KJ204 and the Natural Science Foundation of Shandong Province, grant number ZR2020QF072.

Institutional Review Board Statement: Not applicable.

Informed Consent Statement: Not applicable.

Data Availability Statement: Publicly available datasets were analyzed in this study. These data can be found here: <http://personal-pages.ps.ic.ac.uk/~nina/CSTHSimulation/index.htm>, accessed on 1 December 2022 and <https://sites.ualberta.ca/~bhuang/Stiction-Book.htm>, accessed on 1 December 2022.

Conflicts of Interest: The authors declare no conflict of interest.

Abbreviations

ACF	auto-correlation function
BSD	butterfly-shape-based stiction detection
CNN	convolutional neural network
CSTH	continuous stirred tank heater
DCS	distributed control systems
DFA	detrended fluctuation analysis
DTW	dynamic time warping
DSFA	dynamic slow feature analysis
ISDB	international stiction database
ML	machine learning
ODE	ordinary differential equation
OP	controller output
PV	controlled process variable
PCA	principal component analysis
PSD	power spectral density
SFA	slow feature analysis
SF	slow feature
SVD	singular value decomposition
SDN	stiction detection network
SVM	support vector machines

References

- Sun, Y.; Wu, J.; Xu, J.; Bai, X. Flow Characteristics Study of High-Parameter Multi-Stage Sleeve Control Valve. *Processes* **2022**, *10*, 1504. [[CrossRef](#)]
- Akavalappil, V.; Radhakrishnan, T.K. Comparison of current state of control valve stiction detection and quantification techniques. *Trans. Inst. Meas. Control* **2022**, *44*, 562–579. [[CrossRef](#)]
- Xu, H.; Li, Y.; Zhang, L. A new control method for backlash error elimination of pneumatic control valve. *Processes* **2021**, *9*, 1378. [[CrossRef](#)]
- Damarla, S.K.; Sun, X.; Xu, F.; Shah, A.; Huang, B. Statistical test-based practical methods for detection and quantification of stiction in control valves. *Ind. Eng. Chem. Res.* **2023**, *62*, 4410–4421. [[CrossRef](#)]
- Srinivasan, R.; Rengaswamy, R.; Miller, R. Control loop performance assessment. 1. A qualitative approach for stiction diagnosis. *Ind. Eng. Chem. Res.* **2005**, *44*, 6708–6718. [[CrossRef](#)]
- Choudhury, M.A.A.S.; Thornhill, N.F.; Shah, S.L. Modelling valve stiction. *Control Eng. Pract.* **2005**, *13*, 641–658.
- di Capaci, R.B.; Scali, C. Review and comparison of techniques of analysis of valve stiction: From modeling to smart diagnosis. *Chem. Eng. Res. Des.* **2018**, *130*, 230–265.
- Rossi, M.; Scali, C. A comparison of techniques for automatic detection of stiction: Simulation and application to industrial data. *J. Process Control* **2005**, *15*, 505–514. [[CrossRef](#)]
- Jelali, M.; Huang, B. *Detection and Diagnosis of Stiction in Control Loops*; Springer: London, UK, 2010; p. 391.
- Kayihan, A.; Doyle, F.J. Friction compensation for a process control valve. *Control Eng. Pract.* **2000**, *8*, 799–812. [[CrossRef](#)]
- Li, C.; Qian, F.; Choudhury, M.S.; Du, W. Stiction quantification based on time and frequency domain criterions. In Proceedings of the 9th IFAC Symposium on Advanced Control of Chemical Processes (ADCHEM), Whistler, BC, Canada, 7–10 June 2015; pp. 635–640.
- di Capaci, R.B.; Vaccari, M.; Scali, C.; Pannocchia, G. Enhancing MPC formulations by identification and estimation of valve stiction. *J. Process Control* **2019**, *81*, 31–39. [[CrossRef](#)]
- Romano, R.A.; Garcia, C. Valve friction and nonlinear process model closed-loop identification. *J. Process Control* **2011**, *21*, 667–677. [[CrossRef](#)]
- Karra, S.; Karim, M.N. Comprehensive methodology for detection and diagnosis of oscillatory control loops. *Control Eng. Pract.* **2009**, *17*, 939–956.
- He, Q.P.; Wang, J. Valve stiction quantification method based on a semiphysical valve stiction model. *Ind. Eng. Chem. Res.* **2014**, *53*, 12010–12022.
- Akavalappil, V.; Radhakrishnan, T.K.; Dave, S.K. A convolutional neural network (CNN)-based direct method to detect stiction in control valves. *Can. J. Chem. Eng.* **2023**, *10*, 3963–3981. [[CrossRef](#)]
- Li, S.; Yang, S.H.; Cao, Y. Nonlinear dynamic process monitoring using canonical variate kernel analysis. *Processes* **2022**, *11*, 99.
- Horch, A. A simple method for detection of stiction in control valves. *Control Eng. Pract.* **1999**, *7*, 1221–1231. [[CrossRef](#)]
- Thornhill, N.F.; Huang, B.; Zhang, H. Detection of multiple oscillations in control loops. *J. Process Control* **2003**, *13*, 91–100. [[CrossRef](#)]

20. Yu, W.; Wilson, D.I.; Young, B.R. Nonlinear control performance assessment in the presence of valve stiction. *J. Process Control* **2010**, *20*, 754–761. [[CrossRef](#)]
21. Choudhury, M.A.A.S.; Shah, S.L.; Thornhill, N.F. Diagnosis of poor control-loop performance using higher-order statistics. *Automatica* **2004**, *40*, 1719–1728. [[CrossRef](#)]
22. Garcia, O.P.; Zakharov, A.; Jämsä-Jounela, S.L. Data and reliability characterization strategy for automatic detection of valve stiction in control loops. *IEEE Trans. Control Syst. Technol.* **2016**, *25*, 769–780. [[CrossRef](#)]
23. Zakharov, A.; Zatonni, E.; Xie, L.; Garcia, O.P.; Jämsä-Jounela, S.-L. An autonomous valve stiction detection system based on data characterization. *Control Eng. Pract.* **2013**, *21*, 1507–1518. [[CrossRef](#)]
24. Scali, C.; Ghelardoni, C. An improved qualitative shape analysis technique for automatic detection of valve stiction in flow control loops. *Control Eng. Pract.* **2008**, *16*, 1501–1508. [[CrossRef](#)]
25. Kano, M.; Maruta, H.; Kugemoto, H.; Shimizu, K. Practical model and detection algorithm for valve stiction. In Proceedings of the 7th IFAC Symposium on Dynamics and Control of Process Systems (DYCOPS), Cambridge, MA, USA, 5–7 July 2004; pp. 859–864.
26. Amiruddin, A.A.A.M.; Zabiri, H.; Jeremiah, S.S.; Teh, W.K.; Kamaruddin, B. Valve stiction detection through improved pattern recognition using neural networks. *Control Eng. Pract.* **2019**, *90*, 63–84. [[CrossRef](#)]
27. Henry, Y.Y.S.; Aldrich, C.; Zabiri, H. Detection and severity identification of control valve stiction in industrial loops using integrated partially retrained CNN-PCA frameworks. *Chemom. Intell. Lab. Syst.* **2020**, *206*, 104143. [[CrossRef](#)]
28. Kamaruddin, B.; Zabiri, H.; Amiruddin, A.M.; Teh, W.K.; Ramasamy, M.; Jeremiah, S.S. A simple model-free butterfly shape-based detection (BSD) method integrated with deep learning CNN for valve stiction detection and quantification. *J. Process Control* **2020**, *87*, 1–16. [[CrossRef](#)]
29. Choudhury, M.S.; Shah, S.L.; Thornhill, N.F.; Shook, D.S. Automatic detection and quantification of stiction in control valves. *Control Eng. Pract.* **2006**, *14*, 1395–1412. [[CrossRef](#)]
30. Yamashita, Y. An automatic method for detection of valve stiction in process control loops. *Control Eng. Pract.* **2006**, *14*, 503–510. [[CrossRef](#)]
31. Li, S.; Yang, S.; Cao, Y.; Ji, Z. Nonlinear dynamic process monitoring using deep dynamic principal component analysis. *Syst. Sci. Control Eng.* **2022**, *10*, 55–64. [[CrossRef](#)]
32. Yazdi, Y.A.; Shandiz, H.T.; Narm, H.G. Stiction detection in control valves using a support vector machine with a generalized statistical variable. *ISA Trans.* **2022**, *126*, 407–414. [[CrossRef](#)]
33. Zakharov, A.; Jämsä-Jounela, S.L. Robust oscillation detection index and characterization of oscillating signals for valve stiction detection. *Ind. Eng. Chem. Res.* **2014**, *53*, 5973–5981.
34. Huang, B.; Hu, L.S. A geometrically inspired quantification approach for valve stiction using Riemannian logarithmic map. *Measurement* **2022**, *199*, 111562. [[CrossRef](#)]
35. Teh, W.K.; Zabiri, H.; Samyudia, Y.; Jeremiah, S.S.; Kamaruddin, B.; Amiruddin, A.A.M.; Ramli, N. An improved diagnostic tool for control valve stiction based on nonlinear principle component analysis. *Ind. Eng. Chem. Res.* **2018**, *57*, 11350–11365. [[CrossRef](#)]
36. Chu, F.; Hao, L.L.; Shang, C.; Liu, Y.; Wang, F.L. Assessment of process operating performance with supervised probabilistic slow feature analysis. *J. Process Control* **2023**, *124*, 152–165. [[CrossRef](#)]
37. Shang, L.; Wang, Y.; Deng, X.; Cao, Y.; Wang, P.; Wang, Y. A model predictive control performance monitoring and grading strategy based on improved slow feature analysis. *IEEE Access* **2019**, *7*, 50897–50911. [[CrossRef](#)]
38. Zhang, H.; Tian, X.; Deng, X.; Cao, Y. Batch process fault detection and identification based on discriminant global preserving kernel slow feature analysis. *ISA Trans.* **2018**, *79*, 108–126.
39. Zhang, H.; Li, C.; Li, D.; Zhang, Y.; Peng, W. Fault detection and diagnosis of the air handling unit via an enhanced kernel slow feature analysis approach considering the time-wise and batch-wise dynamics. *Energy Build.* **2021**, *253*, 111467. [[CrossRef](#)]
40. Puli, V.K.; Huang, B. Variational bayesian approach to nonstationary and oscillatory slow feature analysis with applications in soft sensing and process monitoring. *IEEE Trans. Control Syst. Technol.* **2023**, *31*, 1708–1719. [[CrossRef](#)]
41. Wang, J.; Zhao, C. Variants of slow feature analysis framework for automatic detection and isolation of multiple oscillations in coupled control loops. *Comput. Chem. Eng.* **2020**, *141*, 107029.
42. Vogl, M. Hurst exponent dynamics of S & P 500 returns: Implications for market efficiency, long memory, multifractality and financial crises predictability by application of a nonlinear dynamics analysis framework. *Chaos Soliton. Fract.* **2023**, *166*, 112884.
43. Khosroshahi, M.; Poshtan, J.; Alipouri, Y. Practical control performance assessment method using Hurst exponents and crossover phenomena. *Comput. Chem. Eng.* **2022**, *161*, 107774. [[CrossRef](#)]
44. Millen, S.; Beard, R. Estimation of the Hurst exponent for the Burdekin River using the Hurst-Mandelbrot rescaled range statistic. In Proceedings of the First Queensland Statistics Conference, Toowoomba, Australia, 1–3 October 2003.
45. Thornhill, N.F.; Patwardhan, S.C.; Shah, S.L. A continuous stirred tank heater simulation model with applications. *J. Process Control* **2008**, *18*, 347–360. [[CrossRef](#)]
46. Amin, M.T.; Khan, F.; Ahmed, S.; Imtiaz, S. A data-driven Bayesian network learning method for process fault diagnosis. *Process Saf. Environ. Prot.* **2021**, *150*, 110–122. [[CrossRef](#)]
47. Bai, Y.; Zhao, J. A novel transformer-based multi-variable multi-step prediction method for chemical process fault prognosis. *Process Saf. Environ. Prot.* **2023**, *169*, 937–947.

48. Zhang, S.; Qiu, T. Semi-supervised LSTM ladder autoencoder for chemical process fault diagnosis and localization. *Chem. Eng. Sci.* **2022**, *251*, 117467. [[CrossRef](#)]
49. Amin, M.T.; Khan, F.; Halim, S.Z.; Pistikopoulos, S. A holistic framework for process safety and security analysis. *Comput. Chem. Eng.* **2022**, *165*, 107963.

Disclaimer/Publisher's Note: The statements, opinions and data contained in all publications are solely those of the individual author(s) and contributor(s) and not of MDPI and/or the editor(s). MDPI and/or the editor(s) disclaim responsibility for any injury to people or property resulting from any ideas, methods, instructions or products referred to in the content.